



OPEN

Radon concentration in seawater as a geochemical indicator of submarine fault activity in the Yatsushiro Sea, Japan

Kuniyo Kawabata^{1✉}, Fumiaki Tsunomori², Yujin Kitamura³, Yen-Yu Lin^{4,5,6}, Chung-Han Chan^{4,5,6} & Kuo-Fong Ma^{5,7}

This study examined the relationship between radon (^{222}Rn) concentrations in seawater and crustal activity in the Yatsushiro Sea by investigating the submarine fault zone situated at the southern end of the Futagawa–Hinagu fault zone, activated by the 2016 Kumamoto earthquake (M7.3). We conducted an analysis of ^{222}Rn concentration in samples of bottom water just above the seafloor and pore water in sediments, utilizing multiple and piston cores from the *Hakuho Maru* Expedition KH18-3. The findings revealed significantly elevated ^{222}Rn concentrations in the central sites of the Yatsushiro Sea, coinciding with a high-stress field exhibiting dense active faults. Seismicity analysis revealed heightened moment release and a low b-value post the 2016 Kumamoto earthquake, indicative of increased seismic activity and the potential for substantial earthquakes in the Yatsushiro Sea vicinity. Our results indicate that heightened concentrations of ^{222}Rn in seawater can serve as an effective tracer for identifying and estimating submarine fault activities. Moreover, our research highlights the utility of ^{222}Rn concentrations in detecting active submarine faults and assessing their activity. It contributes to a comprehensive understanding of the potential for significant earthquakes in the Yatsushiro Sea in the future.

Radon-222 (^{222}Rn) is a naturally occurring radioactive noble gas, formed in an intermediate step in the radioactive uranium decay chain. ^{222}Rn is highly soluble in water, which allows it to move freely with groundwater and fluids within the Earth's crust. The release rate of ^{222}Rn is primarily contingent on radium-226 concentration in rocks and the surface area of rocks/minerals¹. Variations in surface area, influenced by factors such as porosity, cracks, and fractures, impact the contact area between pore fluid (water or air) and rock, thereby influencing the release of ^{222}Rn . Consequently, the ^{222}Rn concentration can serve as a tracer for determining subsurface rock types and providing insights into groundwater aquifers.

^{222}Rn has been recognized as a precursor of earthquakes and an indicator of crustal deformation^{2–7}. Recently, monitoring networks have been established for soil ^{222}Rn in Italy and China. Machine learning techniques have been applied to analyze the collected data, marking a recent advancement^{8,9}. Active faults, often maturing into well-defined structures with gouge in the fault core, cataclasite, and fracture zones, exhibit an exceptionally high specific surface area in the damaged zone, e.g., $3.3 \times 10^6 \text{ m}^2$ per unit area of the fault surface¹⁰. Water in the crust, such as groundwater and hot springs selectively traverse permeable zones, turning fault zones into conduits for groundwater. The concentration of ^{222}Rn in the crust, especially in groundwater, is a powerful indicator of active faults, allowing for the estimation of fault activity. By mapping ^{222}Rn in groundwater, Tsunomori¹¹ identified large active faults and concluded that the faults may be larger than previously estimated. Furthermore, a correlation between ^{222}Rn concentration and stress evolution was discerned through spatiotemporal variations before and

¹Center for General Education, Kagoshima University, 1-21-30 Korimoto, Kagoshima-City, Kagoshima 890-0082, Japan. ²Geochemical Research Center, Graduate School of Science, The University of Tokyo, 7-3-1 Hongo, Bunkyo-ku, Tokyo 113-0033, Japan. ³Graduate School of Science and Engineering, Kagoshima University, 1-21-35 Korimoto, Kagoshima-City, Kagoshima 890-0082, Japan. ⁴Department of Earth Sciences, National Central University, No.300, Zhongda Rd., Zhongli, Taoyuan 320317, Taiwan. ⁵Earthquake-Disaster and Risk Evaluation and Management (E-DREaM) Center, National Central University, No.300, Zhongda Rd., Zhongli, Taoyuan 320317, Taiwan. ⁶Graduate Institute of Applied Geology, National Central University, No.300, Zhongda Rd., Zhongli, Taoyuan 320317, Taiwan. ⁷Institute of Earth Sciences, Academia Sinica, 128, Sec. 2, Academia Road, Nangang, Taipei 11529, Taiwan. ✉email: kuniyok@km.kagoshima-u.ac.jp

after a large earthquake¹². These investigations mapped groundwater ^{222}Rn concentration on land, revealing active fault locations and estimating their activity. However, the variations in ^{222}Rn concentration around submarine faults have never been reported or discussed. In this study, we attempted to generate a ^{222}Rn concentration map for the Yatsushiro submarine faults, believed to have been activated by the 2016 Kumamoto earthquake. This report presents the ^{222}Rn concentration findings and discusses the relationship between ^{222}Rn concentration and seismicity in the vicinity of the submarine faults.

Yatsushiro submarine faults and sampling

The Yatsushiro submarine faults constitute an active fault group situated in the Yatsushiro Sea, southwest of Kyushu, Japan. This fault network represents the southernmost segment of the Futagawa-Hinagu fault zone, the epicenter of the 2016 Kumamoto Earthquake^{13,14} (Fig. 1). Earthquakes larger than M6.0 have repeatedly occurred in this Yatsushiro Sea segment, raising concerns regarding the potential hazard of another large seismic event in the near future¹⁵.

Historical seismic activities in the Yatsushiro Sea segment date back to 744 and 1619 AD^{16,17}, documented through seafloor acoustic surveys and sedimentary rock dating^{14,18}. The Yatsushiro submarine faults exhibit a steep to nearly vertical orientation, with discernible folding structures in the jog sections connecting the Yatsushiro Sea segment to the adjacent Hinagu segment¹⁸. A seismicity pattern analysis post the 2016 Kumamoto earthquake indicates that the jog section is under high-stress status¹⁹, suggesting an elevated potential for a large earthquake in the area, given the high seismicity rate and active crustal deformation.

The Hakuho Maru Expedition KH18-3 research cruise, conducted from July 27th to 30th, 2018, aimed to elucidate seafloor environmental changes resulting from active faults and submarine landslides triggered by

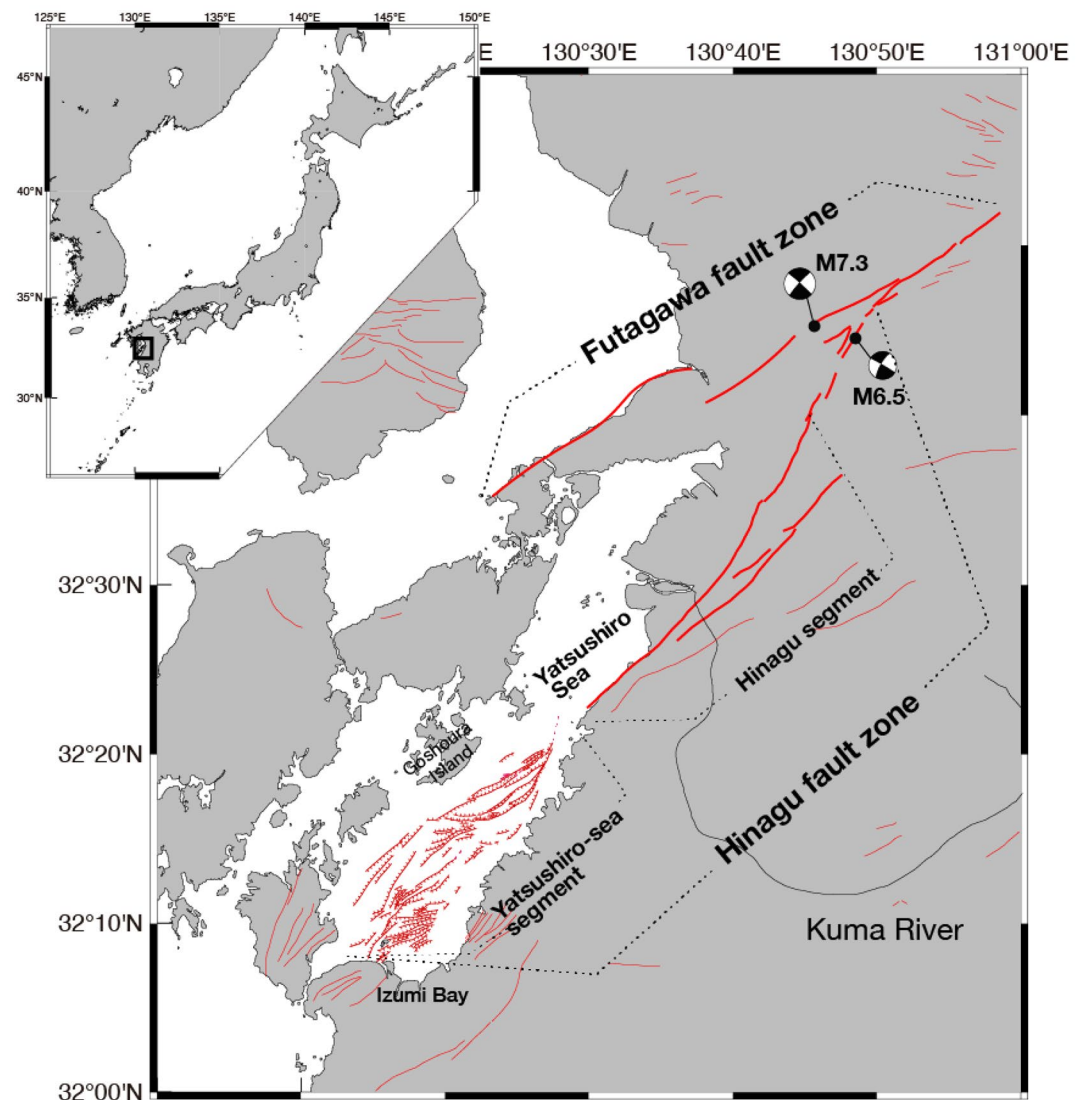


Figure 1. Map of active faults around the Yatsushiro Sea. Red solid and dashed lines show active faults on land and submarine active faults, respectively. Black circles with focal mechanism solutions represent the epicenters of the 2016 Kumamoto earthquakes. The map was generated using Generic Mapping Tools (GMT), ver.6.5²⁸.

the 2016 Kumamoto Earthquake in the Yatsushiro Sea. Additionally, the expedition sought to create a ^{222}Rn concentration map for the Yatsushiro submarine faults. During the expedition, we collected two types of cores using a multiple corer and a piston corer, strategically positioned directly above or near active submarine faults. The multiple corer retrieved sediments below the seafloor in one-meter tubes, accompanied by seawater just above the seafloor, referred to as bottom water. Upon retrieval of the multiple corer onto the deck, the seawater was sampled to measure the ^{222}Rn concentration. For deeper sediment sampling, a long piston corer was employed. In the piston cores, we collected upwelling pore water, which was obtained by self-loading and accumulated at the core's top after standing for a day. Subsequently, the ^{222}Rn concentrations in the piston core water were measured.

Seismicity around Yatsushiro Sea

To analyze the seismicity in the Yatsushiro Sea, earthquake parameters (event location and magnitude) were collected from the earthquake catalog of the Japan Meteorological Agency spanning from January 1996 to February 2020. Seven circular observation regions (regions 1–7) were delineated along the central axis of the Yatsushiro Sea, each possessing a 5 km radius (Fig. 2a). These circular regions exhibited an approximate 5-km overlap in radius with their nearest counterparts, collectively covering the majority of the Yatsushiro Sea. A total of 1853, 1719, 1731, 1338, 1687, 1740, and 1027 earthquakes were incorporated into our calculations for regions 1–7, respectively.

Utilizing this dataset, the b -value and moment release for the specified regions were determined, as outlined in the Method section. Figures 2b, c and d, along with S1, summarize the b -value, moment release, and event count over the entire period. Regions 2 and 3 exhibited lower b -values and higher moment release. Given the substantial seismic event count in each zone, the associated uncertainty in b -value calculation is comparatively

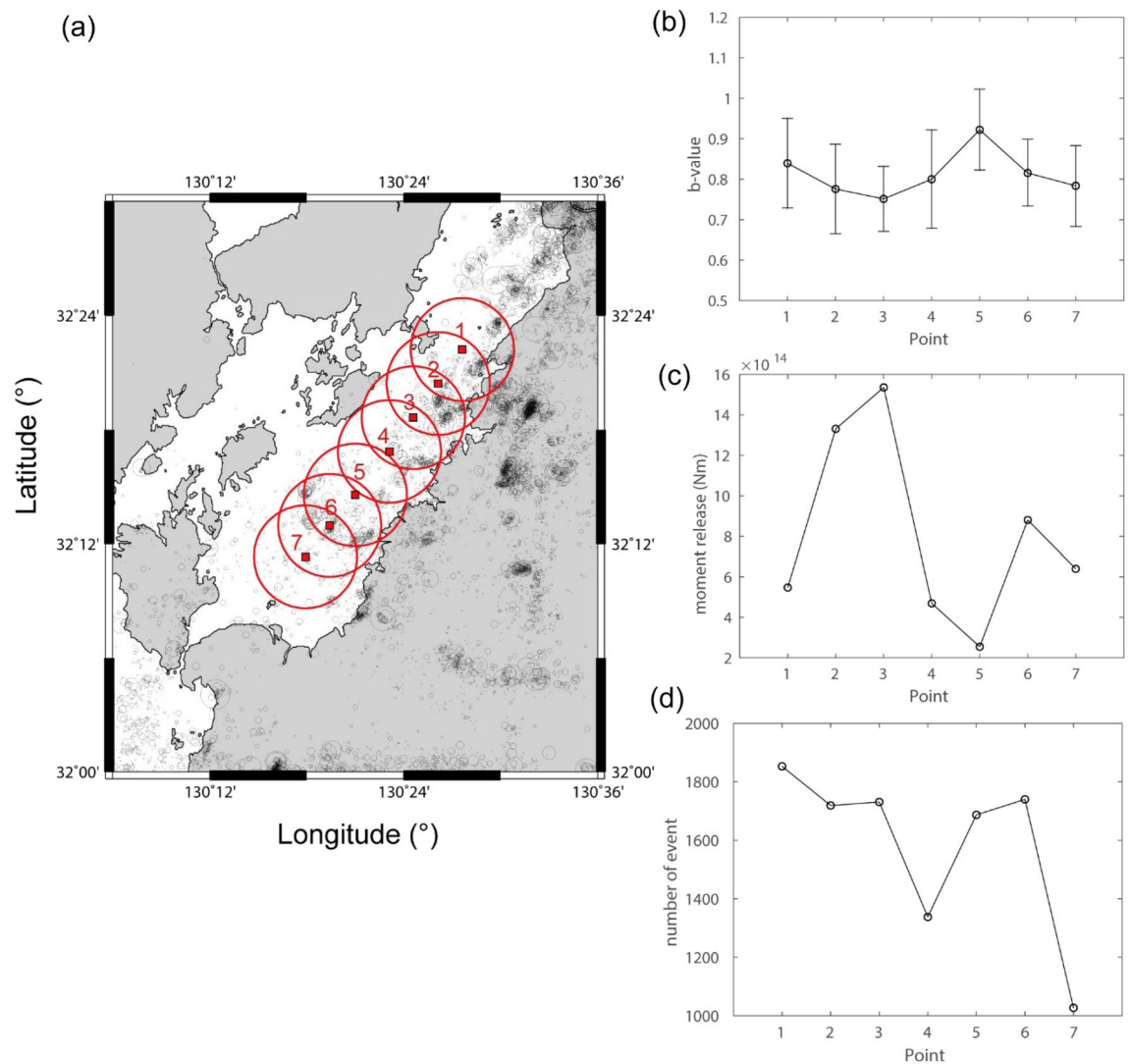


Figure 2. (a) Regions where the seismicity study was conducted. The red circles indicate the six regions for the seismicity investigation along the Yatsushiro Sea. Analysis results showcasing (b) b -value, (c) moment release, and (d) event count for each specified region. The map was prepared using GMT, ver.6.5²⁸.

low. Specifically, when considering both the b -value and event count, the standard deviation of the b -value ranges from 0.018 to 0.024, a range significantly smaller than the temporal variations observed in b -values. Notably, the central area in the Yatsushiro Sea, encompassing regions 2 and 3, displayed heightened seismic activity. These results suggest that regions 2 and 3 may possess heightened potential for stress accumulation.

Further analysis was conducted on seismic data pre and post the 2016 Kumamoto earthquake (Figs. 3, S2, S3). Following the earthquake, there were noticeable changes in the spatial distribution of b -value and moment release were observed. Specifically, b -values in regions 2 and 3 decreased post-earthquake. A higher moment release was observed in the southern area (regions 6 and 7) before the earthquake, whereas post-earthquake, the central area (regions 2 and 3) exhibited heightened moment release. These findings indicate an intensified crustal deformation process, including increased seismic activity in the central area of the Yatsushiro Sea, subsequent to the 2016 Kumamoto earthquake.

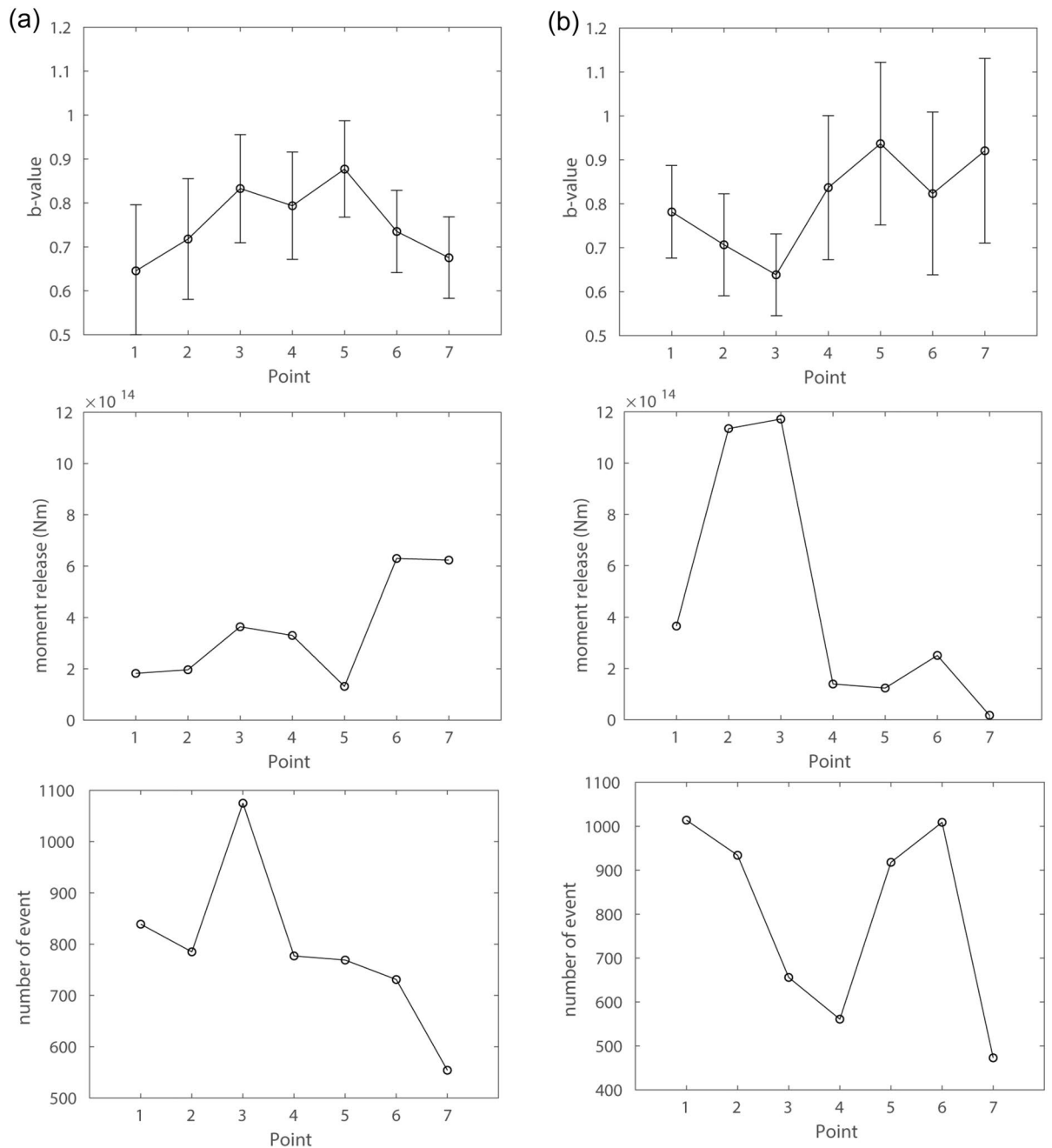


Figure 3. Analysis results showcasing b -value, moment release, and event count for each specified area (a) before and (b) after the 2016 Kumamoto earthquake.

Results for core analysis and ^{222}Rn concentrations

Results obtained from the examination of piston cores are depicted in Fig. 4 and Supplementary Fig S4. The sediment composition in the Yatsushiro Sea primarily includes mud and sand, along with some volcanoclastics. In the southwestern region of the Yatsushiro Sea, conglomerate beds were observed at sites PC7 and PC10 (Fig. S4 a–e). Cores, especially those with conglomerate layers, exhibit a higher presence of upwelling water. Within the conglomerate layer of PC 10, minor granitoid gravels were detected, predominantly consisting of sandy gravels. These granules likely originate from Goshoura Island, located to the northwest of PC10, where Granodiorite is partially exposed in sedimentary rocks. Sediments obtained by multiple cores consist entirely of soft mud (Fig. S4 f.). The mud collected from all sampling locations is similar.

The concentration of ^{222}Rn in seawater samples obtained using multiple cores (MC) and piston cores (PC) was measured. ^{222}Rn concentrations were determined using a radon and thron monitor (RTM 1688, SARAD GmbH, Germany) attached to a gas–water separation bottle (Fig. S5). The detailed measurement technique is discussed in the Methods section.

Results of ^{222}Rn concentrations for the MC and PC samples are illustrated in Fig. 5a and b and Table S1. The ^{222}Rn concentrations in the PC samples surpassed those in the MC samples, with notably higher concentrations in sediments containing conglomerate layers.

Typically, ^{222}Rn is rarely detected in seawater. However, we observed ^{222}Rn concentrations in bottom water (MC samples), particularly at sites MC7, 8, 9, 11, and 12, where relatively high ^{222}Rn concentrations were noted. MC12 and PC10 represent the same sites, both containing a thick conglomerate layer. The central area in the Yatsushiro Sea around sites MC7, 8, 9, and 11 is a region exhibiting high ^{222}Rn concentrations despite the absence of conglomerate beds. The high ^{222}Rn concentration regions around MC7, 8, 9, and 11 align with the area seismically most active (2 and 3). The area is situated close to the segment boundary between the Yatsushiro Sea segment and the Hinagu segment (Fig. 1), and the region is considered to be under high stress^{18,19}. The high-stress condition can also be inferred from geological structures such as pressure ridge formations and their displacement by active faults in the area¹⁸.

Discussion

High concentrations of ^{222}Rn in bottom water were observed at sites above conglomerate beds and in high-stress condition areas near the boundary between the Yatsushiro Sea and the Hinagu segments. Various factors may influence the ^{222}Rn concentration in bottom water, including (1) different radium concentrations in rock types, (2) water flow from terrestrial sources, (3) water flow rates from sediments, and (4) crustal deformation involving changes in porosity and/or fracture formation¹.

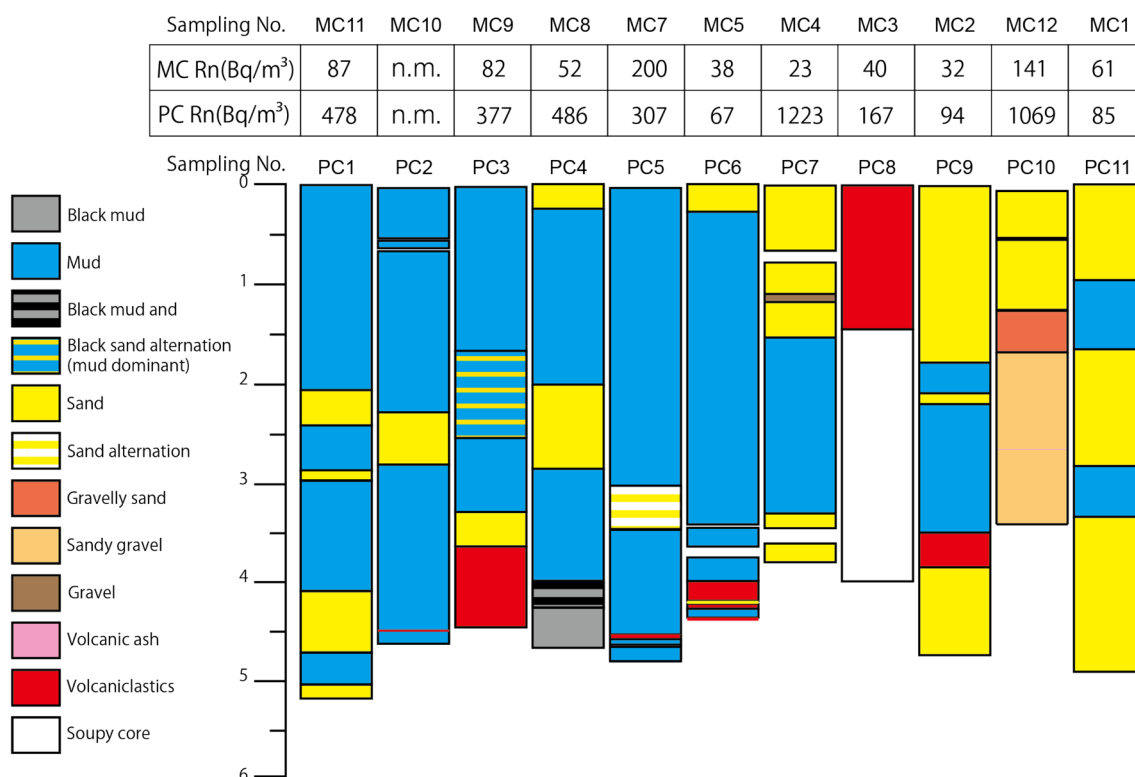


Figure 4. Geological columnar sections of piston core (PC) and corresponding ^{222}Rn concentrations (PC samples) and bottom water samples from nearly the same location (multiple core (MC) samples). “n.m.” indicates that the measurement was not conducted due to the inability to obtain the seawater samples. Conglomerate layers are observed in cores from sites PC7 and PC10.

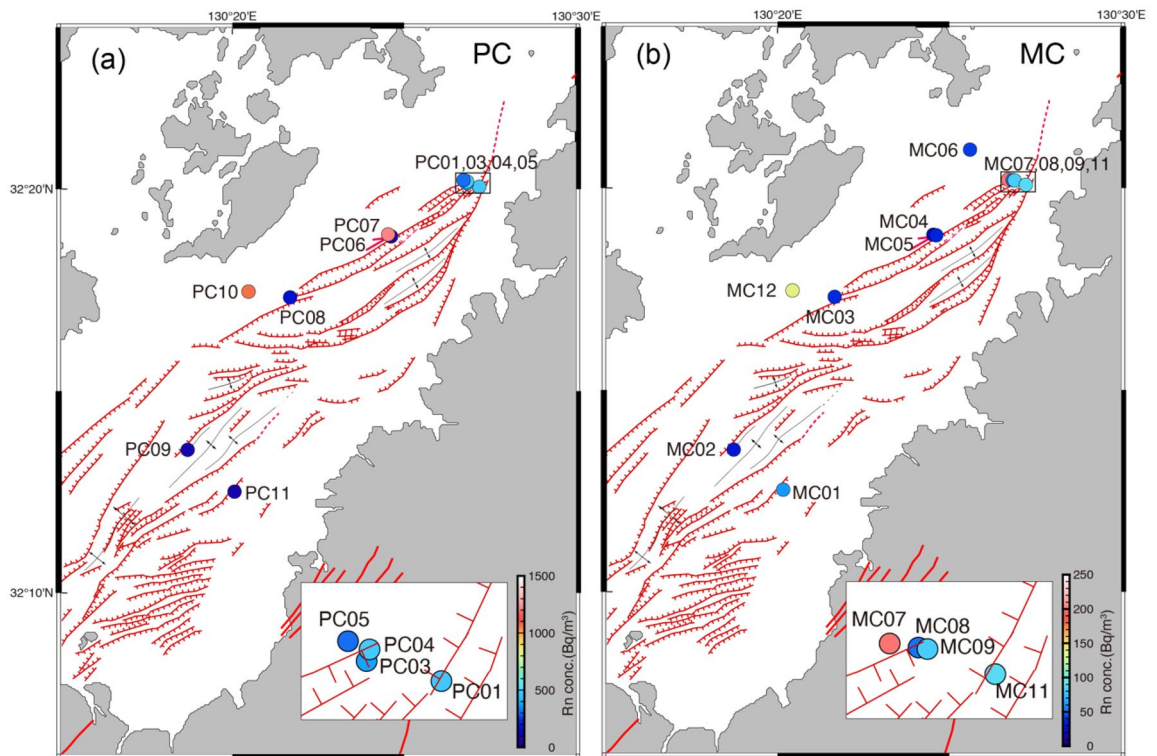


Figure 5. Results of ^{222}Rn concentration measurements around Yatsushiro submarine faults¹⁴ in (a) upwelling water from piston core (PC) and (b) bottom water from multiple core (MC). The map was generated using GMT, ver.6.5²⁸.

The amount of radium-226, which decays into ^{222}Rn , in host sediments varies based on mineral composition. However, the sediments beneath the Yatsushiro Sea are quasi-homogeneous²⁰, with a minor presence of granitic rock only in the gravel layer of PC10, which could contain a relatively high concentration of uranium-238. Therefore, the observation results suggest that the higher ^{222}Rn concentration is not solely attributed to differences in rock types. The sample containing a conglomerate layer, PC10, may slightly elevate ^{222}Rn concentration.

The primary source of terrestrial water in the region is the Kuma River, the only major river flowing into the Yatsushiro Sea (Fig. 1). Nikpeyman et al.²¹ noted that the ^{222}Rn concentration in water discharged from the Kuma River is relatively high along the coastal region near the estuary of the Kuma River in the Yatsushiro Sea. Higher ^{222}Rn concentrations were observed in Izumi Bay on the southern side of the Yatsushiro Sea, attributed to submarine groundwater discharge (SGD). However, the offshore regions of the Yatsushiro Sea show minimal impact from ^{222}Rn originating from both the Kuma River and SGD in Izumi Bay. In addition to measuring ^{222}Rn concentrations, they conducted simulations to assess the seasonal influence of ^{222}Rn , including the spread of river water discharging from the sea surface to the seabed. Simulation results confirm that ^{222}Rn from the river predominantly affects the northern area of the Yatsushiro Sea. Our sampling locations, situated in the central and southern regions of the Yatsushiro Sea at a depth of around 50 m, receive negligible ^{222}Rn contribution from terrestrial water.

Crustal deformation plays a pivotal role in the release of ^{222}Rn through alterations in permeability and specific surface area induced by crack formation and fracturing. The fracture zone, encompassing cracks and fractured grains, exhibits a higher water–rock contact area compared to the host rock²². Fault zones with flowing water display elevated ^{222}Rn concentrations due to increased release from rocks into the surrounding water¹¹. Permeability changes resulting from stress-induced crack formation can also influence the flow rate of upwelling water, leading to the discharge of highly concentrated ^{222}Rn water onto the seafloor.

Both MC and PC samples indicate that conglomerate beds tend to induce higher ^{222}Rn concentrations. These conglomerate layers, characterized by high porosity and increased water content in the pore space, undergo compaction, facilitating the easy upwelling of pore water with elevated concentrations of ^{222}Rn . The observed ^{222}Rn concentration and related results align with water flowing through porous conglomerate sediments. The flow rate in conglomerates, with higher permeability and porosity compared to muddy and sandy sediments, would be faster. The steady state concentration of ^{222}Rn in bottom water at the seafloor is maintained by inflow from sediments, outflow due to migration and diffusion in the bottom water, and its decay. The faster flow of a larger volume of pore water through conglomerates results in a higher supply of ^{222}Rn to bottom water than in sediments without conglomerates. The ^{222}Rn concentration at site MC 12, including conglomerates, would be higher due to faster upwelling through porous sediments. Minor granitoid gravels around PC10 and MC12 may also contribute to increased ^{222}Rn levels.

In the study area, elevated ^{222}Rn concentrations were observed in the vicinity of sites MC 7, 8, 9, and 11. Sediments around these sites primarily consist of sand and mud, with no conglomerates. ^{222}Rn from river water is negligible around the area. However, the region with higher ^{222}Rn concentration aligns with a large number of seismic events, high moment releases and low b -values (Fig. 2), indicative of seismically active and higher stress concentration. Continuous release of ^{222}Rn by seismic events, passing through a highly permeable fault zone with water to the seafloor, could contribute to the observed ^{222}Rn levels. Following the 2016 Kumamoto earthquake, a notable increase in both the number of seismic events and moment release occurred in the vicinity (Fig. 3). Considering the half-life of ^{222}Rn (3.8 days), our measurements reflect the crustal condition after the 2016 Kumamoto earthquake. The heightened seismic activity likely played a role in the increased in-water ^{222}Rn levels observed in the central area of the Yatsushiro Sea, specifically around sites MC 7 through 11, suggesting a potential post-earthquake influence on ^{222}Rn concentration in the region.

This study establishes the relationship between crustal activity and ^{222}Rn concentration. To further validate the correlation between seismic activity and ^{222}Rn levels, regular measurements of radon concentration are imperative. Ongoing monitoring will contribute to a comprehensive understanding of the dynamic interplay between crustal processes and ^{222}Rn release in marine environments.

Conclusion

The investigation of ^{222}Rn concentrations in the bottom water of the Yatsushiro submarine faults has unveiled elevated levels in highly permeable sediments and regions characterized by intense tectonic and seismic activity. An examination of minor seismic events in the Yatsushiro Sea post the 2016 Kumamoto earthquake indicates a heightened seismic activity. It is evident that seismic events led to the release of ^{222}Rn through crack formations, with subsequent movement and upwelling occurring through permeable active faults. Furthermore, the active fault zone itself plays a role in the presence of ^{222}Rn in the passing seawater. These discoveries posit that ^{222}Rn concentrations can serve as an effective indicator of crustal activity not solely on land but also beneath the sea.

Methods

Measurement of in-water ^{222}Rn concentration

The methodology employed for determining the ^{222}Rn concentration in water aligns with that detailed by Kawabata et al.¹² Initially, a 1.0-L volume of seawater was transferred into a 2.2-L bottle, which was subsequently sealed with a screwcap housing two tube connectors (see Fig. S1). To expedite the establishment of gas–liquid equilibrium, the bottled seawater underwent vigorous hand agitation for a duration of three minutes. Following this, the air in the gas phase within the bottle was dehumidified utilizing a DRIERITE® drying column and was then directed into a ^{222}Rn monitor via an internal pump. The ^{222}Rn monitor continuously acquired the energy spectrum of alpha particles emitted by daughter elements of radon-222 over a 15-min period for each measurement. Three consecutive sets of measurements were conducted for each sample, with the maximum values from the second or third measurements deemed as the ^{222}Rn concentration data in the gas phase. This approach accounted for incomplete equilibrium conditions during the initial measurement stage.

We estimated the ^{222}Rn concentration in the aqueous phase by considering the time elapsed from the date of sampling. The equation for the conservation of ^{222}Rn in gas and water in the measurement system is:

$$C_a V_a + C_w V_w = C_a(eq) V_a + C_w(eq) V_w, \quad (1)$$

where C_a and C_w denote the ^{222}Rn concentrations in the gas phase and water phase, respectively, before agitation, and $C_a(eq)$ and $C_w(eq)$ are the ^{222}Rn concentrations in the gas and water phases at equilibrium, respectively; V_a and V_w represent the volumes of the gas and water phase, respectively.

The ^{222}Rn equilibrium constant²³, Kd is expressed as:

$$Kd = \frac{C_w(eq)}{C_a(eq)} = 0.15 + 0.403\exp(-0.0502T) \quad (2)$$

where, by assuming C_a to be 0, we estimated the ^{222}Rn concentration in water prior to measurement (C_w) using Eq. (1):

$$C_w = C_a(eq) \left(\frac{V_a}{V_w} + Kd \right) \quad (3)$$

We calculated ^{222}Rn concentration in water at sampling time, C_{w0} , using the 3.8 d half-life of ^{222}Rn , when measurement start time deviated from the sampling time.

Analysis of seismicity (b -value and moment release)

In our investigation, the determination of the b -value in the study regions followed the Gutenberg–Richter relation²⁴. The frequency–magnitude distribution can be depicted in a seismogenic domain as:

$$\log_{10} N = a - bM, \quad (4)$$

Here, M represents the magnitude, N indicates the number of earthquakes with a magnitude within $M \pm 0.1$, and both a and b are constants determined through regression analysis of seismic activity. The 90% confidence interval for the slope coefficient was interpreted as the uncertainty of the b -value. This parameter signifies the proportion of small to large seismic events, with its variation within a region often reflecting the specific

characteristics of its seismic activity. A low b -value in a region suggests significant differential stress, indicating proximity to the end of its seismic cycle²⁵.

To accurately determine the standard deviation of the b -value, we employed a methodology²⁶ that entails the following steps:

$$\sigma = bN^{-1/2}, \quad (5)$$

where N represents the total number of seismic events utilized for estimating the b -value. Upon examining the b -values depicted in Fig. 2b and the event counts shown in Fig. 2d across regions 1–7, the respective standard deviations (σ) are calculated to be 0.020, 0.019, 0.018, 0.022, 0.022, 0.020, and 0.024, respectively.

Furthermore, we calculated seismic moment of all events in each region and added them up to obtain the moment release. The magnitude–moment relation is

$$M_w = \left(\frac{\log_{10} M_0}{1.5} \right) - 10.73, \quad (6)$$

where M_w is moment magnitude and M_0 is seismic moment in dyne-cm²⁷.

Data availability

All data generated or analyzed during this study are included in this published article (and its Supplementary Information file). The earthquake parameters were collected from the earthquake catalog of the Japan Meteorological Agency (https://www.data.jma.go.jp/svd/eqev/data/bulletin/hypo_e.html).

Received: 27 November 2023; Accepted: 5 April 2024

Published online: 15 April 2024

References

1. United Nations Scientific Committee on the Effects of Atomic Radiation. UNSCEAR 2000 Report to the General Assembly, with Scientific Annexes: Sources and Effects of Ionizing Radiation. I, 97–99 (2000).
2. Wakita, H., Nakamura, Y., Notsu, K., Noguchi, M. & Asada, T. Radon anomaly: a possible precursor of the 1978 Izu–Oshima-kinkai earthquake. *Science* **207**, 882–883 (1980).
3. Igarashi, G. *et al.* Ground-water radon anomaly before the Kobe earthquake in Japan. *Science* **269**, 60–61 (1995).
4. Tsunogai, U. & Wakita, H. Precursory chemical changes in ground water: Kobe earthquake, Japan. *Science* **269**, 61–63 (1995).
5. Tsunomori, F. & Tanaka, H. Anomalous change of groundwater radon concentration monitored at Nakaizu well in 2011. *Radiat. Meas.* **60**, 35–41 (2014).
6. Kuo, T., Chen, W. & Ho, C. Anomalous decrease in groundwater radon before 2016 Mw 6.4 Meinong earthquake and its application in Taiwan. *Appl. Radiat. Isot.* **136**, 68–72 (2018).
7. Zhou, Z., Tian, L., Zhao, J., Wang, H. & Liu, J. Stress-related ore-seismic water radon concentration variations in the Panjin observation well, China (1994–2020). *Front. Earth Sci.* **8**, 1–12 (2020).
8. Cannelli, V., Piersanti, A., Galli, G. & Melini, D. Italian radon monitoring network (Iron): A permanent network for near real-time monitoring of soil radon emission in Italy. *Ann. Geophys.* **61**, 1–22 (2018).
9. Chen, Z. *et al.* Radon emission from soil gases in the active fault zones in the Capital of China and its environmental effects. *Sci. Rep.* **8**, 1–12 (2018).
10. Chester, J. S., Chester, F. M. & Kronenberg, A. K. Fracture surface energy of the Punchbowl fault, San Andreas system. *Nature* **437**, 133–136 (2005).
11. Tsunomori, F., Shimodate, T., Ide, T. & Tanaka, H. Radon concentration distributions in shallow and deep groundwater around the Tachikawa fault zone. *J. Environ. Radioact.* **172**, 106–112 (2017).
12. Kawabata, K. *et al.* Changes in groundwater radon concentrations caused by the 2016 Kumamoto earthquake. *J. Hydrol.* <https://doi.org/10.1016/j.jhydrol.2020.124712> (2020).
13. Chida, N., Okamura, M. & Ogawa, M. A preliminary report on submarine active faults beneath Yatsushiro Bay, Southwest Japan. *Act. Fault Res.* **9**, 93–97 (1991).
14. Kagohara, K. *et al.* High-resolution multi-channel seismic reflection imaging of the Futagawa–Hinagu Fault Zone, Yatsushiro Sea, southwest Japan. *Annu. Rep. Act. Fault Paleoequake Res.* 273–294 (2011).
15. The Headquarters for Earthquake Research Promotion. Evaluation of the Futagawa fault zone and the Hinagu fault zone (partial revision). (2013).
16. Matsuda, T. Collating records in nature and in history: contribution to earthquake prediction. *J. Geog.* **108**, 370–377 (1999).
17. Chida, N. Late quaternary activity of Hinagu fault, west central Kyushu. *Ann. Tohoku Geogr. Assoc.* **31**, 172–179 (1979).
18. Yagi, M. *et al.* Identification of faulting history of active faults in coastal area using high-resolution seismic survey and piston coring: A case study on the offshore extension of the Hinagu Fault Zone in the Yatsushiro Sea. *Act. Fault Res.* **45**, 1–19 (2016).
19. Nanjo, K. Z., Izutsu, J., Orihara, Y., Kamogawa, M. & Nagao, T. Changes in seismicity pattern due to the 2016 Kumamoto earthquakes identify a highly stressed area on the Hinagu fault zone. *Geophys. Res. Lett.* **46**, 9489–9496 (2019).
20. Oki, K. & Tomiyasu, T. Sedimentary environments based on textures of surface sediments and sedimentation rates in the South Yatsushiro Kai (Sea), southwest Kyushu, Japan. *J. Sedimentol. Soc. Japan* **48**, 67–84 (1998).
21. Nikpeyman, Y. *et al.* Assessment of the spatial distribution of submarine groundwater discharge (SGD) along the Yatsushiro Inland Sea coastline, SW Japan, using 222Rn method. *J. Radioanal. Nucl. Chem.* **307**, 2123–2132 (2016).
22. Caine, J. S., Evans, J. P. & Forster, C. B. Fault zone architecture and permeability structure. *Geology* **24**, 1025–1028 (1996).
23. Weigel, F. Radon. *Chem. Ztg.* **102**, 287 (1978).
24. Gutenberg, B. & Richter, C. *Seismicity of the Earth and Associated Phenomena* 2nd edn, 310 (Princeton Univ. Press, 1954).
25. Schorlemmer, D., Wiemer, S. & Wyss, M. Variations in earthquake-size distribution across different stress regimes. *Nature* **437**(22), 539–542 (2005).
26. Aki, K. Maximum likelihood estimate of b in the formula $\log N = a - bM$ and its confidence. *Bull. Earthq. Res. Inst. Univ. Tokyo* **43**, 237–239 (1965).
27. Lay, T. & Wallace, T. C. *Modern global seismology* (Academic Press, 1995).
28. Wessel, P. *et al.* The generic mapping tools version 6. *Geochem. Geophys. Geosyst.* **20**, 5556–5564 (2019).

Acknowledgements

This research used data provided by the *Hakuho Maru* cruises of the KH18-3 Expedition. We would like to thank the scientists of Expedition KH18-3, the operation staff of *Hakuho Maru*, and the onboard laboratory technicians for their invaluable contributions in obtaining samples and data. This study was performed under the cooperative research program of Center for Advanced Marine Core Research, Kochi University (Accept No. 18C005, 19A053, 19B048, 20A060, 20B055). We appreciate Kyoko Kagohara for providing the map data of Yatsushiro submarine faults. Some figures in our paper were prepared using the Generic Mapping Tools²⁸. Additionally, we extend our thanks to the anonymous reviewers whose insightful comments and suggestions significantly elevated the quality of this manuscript.

Author contributions

K. K. and F. T. contributed to the ²²²Rn measurement analysis, Y. K., the chief of the KH18-3 Expedition, contributed to the identification of Geology in the study area and core analysis, and Y.-Y. L, C.-H. C. and K.-F. contributed to the seismicity analyses. All authors contributed to the design of the research, scientific discussion, and writing of the manuscript.

Funding

This study received funding from the MEXT Support Program for the Development of Human Resources in Science and Technology, specifically the “Initiative for realizing diversity in the research environment (Leading-type)”, through fund no. FY2020.

Competing interests

The authors declare no competing interests.

Additional information

Supplementary Information The online version contains supplementary material available at <https://doi.org/10.1038/s41598-024-59006-6>.

Correspondence and requests for materials should be addressed to K.K.

Reprints and permissions information is available at www.nature.com/reprints.

Publisher’s note Springer Nature remains neutral with regard to jurisdictional claims in published maps and institutional affiliations.



Open Access This article is licensed under a Creative Commons Attribution 4.0 International License, which permits use, sharing, adaptation, distribution and reproduction in any medium or format, as long as you give appropriate credit to the original author(s) and the source, provide a link to the Creative Commons licence, and indicate if changes were made. The images or other third party material in this article are included in the article’s Creative Commons licence, unless indicated otherwise in a credit line to the material. If material is not included in the article’s Creative Commons licence and your intended use is not permitted by statutory regulation or exceeds the permitted use, you will need to obtain permission directly from the copyright holder. To view a copy of this licence, visit <http://creativecommons.org/licenses/by/4.0/>.

© The Author(s) 2024